ELSEVIER

Contents lists available at ScienceDirect

Nuclear Inst. and Methods in Physics Research, A

journal homepage: www.elsevier.com/locate/nima



Full Length Article

Performance of modular ring imaging Cherenkov detector for particle identification

D. Sharma ^a, L. Barion ^b, M. Contalbrigo ^b, K. Gnanvo ^c, X. He ^a, Y. Ilieva ^d, B. Karki ^e, M. Sarsour ^{a,*}, Z.W. Zhao ^e

- ^a Department of Physics and Astronomy, Georgia State University, Atlanta, GA 30303, USA
- ^b INFN Sezione di Ferrara, 44122 Ferrara, Italy
- ^c Thomas Jefferson National Accelerator Facility, Newport News, VA 23606, USA
- ^d University of South Carolina, Columbia, SC 29208, USA
- e Department of Physics, Duke University, Durham, NC 27708, USA

ARTICLE INFO

Keywords: RICH - Ring Imaging Cherenkov EIC - Electron Ion Collider PID - Particle Identification Fresnel lens Aerogel

ABSTRACT

A compact modular ring imaging Cherenkov (mRICH) detector has been developed to provide K/π separation over a momentum coverage of 2 to 10 GeV/c, and an e/π separation of up to 2.5 GeV/c within the Electron-Ion Collider Generic R&D Consortium (i.e., eRD14 Collaboration). The mRICH detector consists of an aerogel block, a Fresnel lens, a flat-mirror set, and a photosensor plane. In September 2021, an mRICH beam-test was carried out at Jefferson Laboratory (JLab). In this paper, results from JLab beam test will be presented together with future plans for mRICH R&D activities.

1. Introduction

Excellent particle identification (PID) is an essential requirement for the future Electron Ion Collider (EIC) experiments [1-3]. PID of the final state hadrons in the semi-inclusive deep inelastic scattering allows the measurement of flavor-dependent quark and gluon distributions inside nucleons and nuclei. The EIC PID Consortium (eRD14 Collaboration) was formed in 2015 for identifying and developing PID detectors using ring imaging Cherenkov (RICH) and ultra-fast time-offlight (TOF) techniques for the EIC experiments with a broad kinematic coverage. The ring imaging Cherenkov detectors provide particle identification over a wide momentum range from a few GeV/c up to 10's of GeV/c with the proper choices of radiator materials. For the momentum coverage between 2 GeV/c to 10 GeV/c, the aerogel-based RICH detector is the only viable PID solution. The current technologies being used are either proximity focusing [4,5], or mirror based imaging, and require a substantial detector volume. A compact modular ring imaging Cherenkov (mRICH) detector has been developed to fulfill the PID and space requirements.

The successful development of the mRICH detector technology started in 2014. Two beam tests were carried at Fermi National Accelerator laboratory (FNAL) in 2016 and 2018, respectively, that led to a mature mRICH prototype design. They provided a proof of principle (lens focusing) and demonstrated the design features of mRICH [6]. The novel design of mRICH consists of four components. A 3.0 cm

thick aerogel block with index of refraction n = 1.03, a Fresnel lens with 15.24 mm (6") focal length, and a sensor plane composed of four Hamamatsu H13700-03 (3 mm \times 3 mm pixel size) multianode PMTs. The gap between the lens and the image plane is bounded by four flat mirrors. All these components including readout electronics add up to 30 cm longitudinally, which is far less than required for proximity focusing design. Fig. 1(a) shows the working principle of mRICH. Also shown in Fig. 1(b) is an mRICH event display of a 5 GeV/c pion from a realistic GEANT4 [7] simulation. A 3D illustration of the main detector components is shown in Fig. 1(c).

In this paper, we present the results from the mRICH beam test at the Jefferson Laboratory (JLab). This test included a pair of GEM trackers which allows us to extract the Cherenkov angle resolution and to study the aerogel edge effect on the properties of the ring image patterns on the photosensor plane.

2. Test setup at JLab

This beam test was performed in Hall D at JLab. The setup was installed downstream of the pair spectrometer, as shown in Fig. 2. Electron–positron pairs are created by beam of photons inside a thin converter with a typical thickness ranging between 10^{-4} to 10^{-2} radiation lengths. The produced electron–positron pairs are deflected

E-mail address: msar@gsu.edu (M. Sarsour).

^{*} Corresponding author.

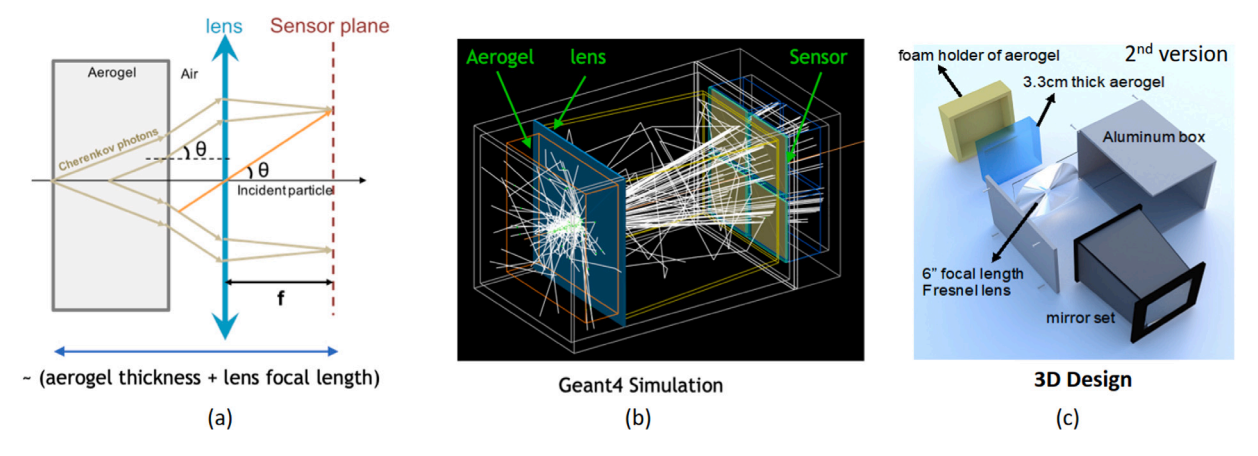


Fig. 1. (a) Conceptual ray-diagram of the mRICH working principle; (b) Detector and an event display from GEANT4 simulation; (c) 3D illustration of the mRICH components.

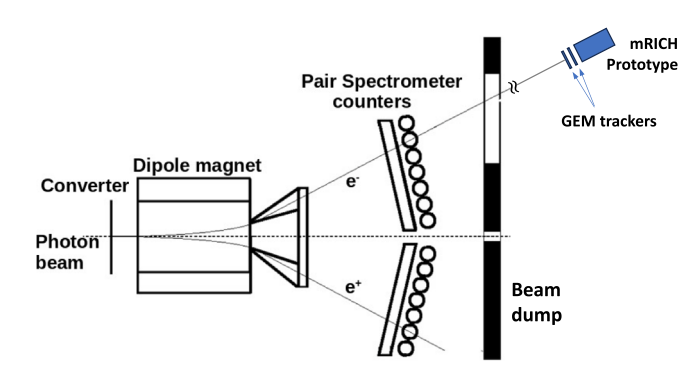


Fig. 2. mRICH beam test setup in Hall-D at JLab.

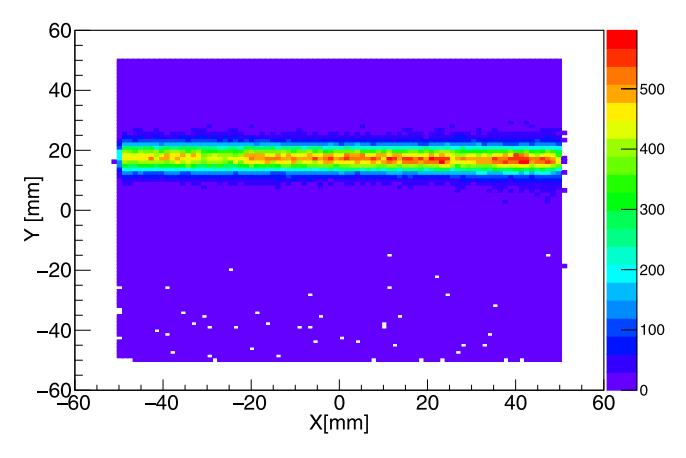


Fig. 3. Beam hits distribution reconstructed from the front GEM tracker.

in a dipole magnet with an effective field length of about 0.94 m. The mRICH setup was installed along the electron arm. The electron momentum produced from the pair spectrometer ranges from 1 to 6 GeV/c. The beam profile forms a horizontal band of ± 5 cm in X and 1 cm in Y, as shown in Fig. 3. The central line of the incident electron band lies at about 1.5 cm above the center of mRICH module. The shift gives us a unique opportunity to study the edge effect of the aerogel block on the Cherenkov ring image formation and efficiency estimation. Two small standard (10 cm \times 10 cm) triple-GEM trackers with COMPASS readout [8], consisting of 256 strips each in X and Y directions, were positioned upstream of mRICH prototype to provide tracking. The GEM trackers were read out by the APV25-based [9]

Scalable Readout System (SRS) [10], with 2 APV25 front end (FE) boards per X-Y-strip plane of each detector. The signal for a given channel consisted of six time-samples of the APV25 waveform signal. For clarity and consistency, we will refer to the two GEMs as GEM0 and GEM1, with GEM1 closer to mRICH module. The signals from mRICH's four Hamamatsu H13700 PMTs were read out with electronics provided by the INFN Ferrara group [6].

3. Data analysis

The analysis starts with selecting a valid electron track that is defined as having matched hits in the two GEMs. The bias voltages on the GEMs were set so that each GEM retains a hit reconstruction efficiency close to 97%. The matching window to form a track was set to \pm 1.5 mm in both the X and Y directions. This window was determined from the distributions of X (and Y) hit positions in both GEMs and it roughly corresponds to 3σ of the obtained distribution. Following each track, we perform a straight line projection of the track onto the face of the aerogel block in mRICH. This projection also allows us to associate the beam hit spot on the photosensor plane of mRICH. The cluster of the pixel hits which are associated with the beam spot is excluded in determining the ring image.

Typical noise sources include photons from Rayleigh scattering inside the aerogel block, Cherenkov photons from the Fresnel lens and from the sensor glass windows, and possibly from the back-scattered particles from the sensor electronics produced by the incident beam particles. The noise hits from the Rayleigh scattering inside the aerogel block and the Cherenkov photons from Fresnel lens generate random and uniform hits on the sensor plane. Cherenkov photons generated inside the PMT glass window and the noise hits from the back-scattered particles tend to be close to the spot where the beam particles hit because of the short distance among these components. We have implemented these noise sources in the simulation.

Examples of cumulative rings are shown in Fig. 4. Each panel shows a 1 mm bin in the X-projection (X_{Proj}) for a few representative spots along the horizontal beam position. The corresponding Y-projection (Y_{Proj}) bin is between 15 to 16 mm. The ring image is fitted by an ellipse since it is not a perfect circle due to several factors including the sensor location not being at the optimal focusing position, incidence angle of the track on the aerogel and its proximity to edge of the aerogel block.

For one given event and a given track position on mRICH as determined using the GEMs, the corresponding associated cumulative ring fit parameters are used as initial seed parameters for fitting the hits resulting from the event. All the hits that are more than 4σ away from the cumulative ring radius are removed, where σ is the uncertainty associated with the cumulative image fit parameters. The remaining photon hits are fitted with an ellipse and an iterative fit procedure is

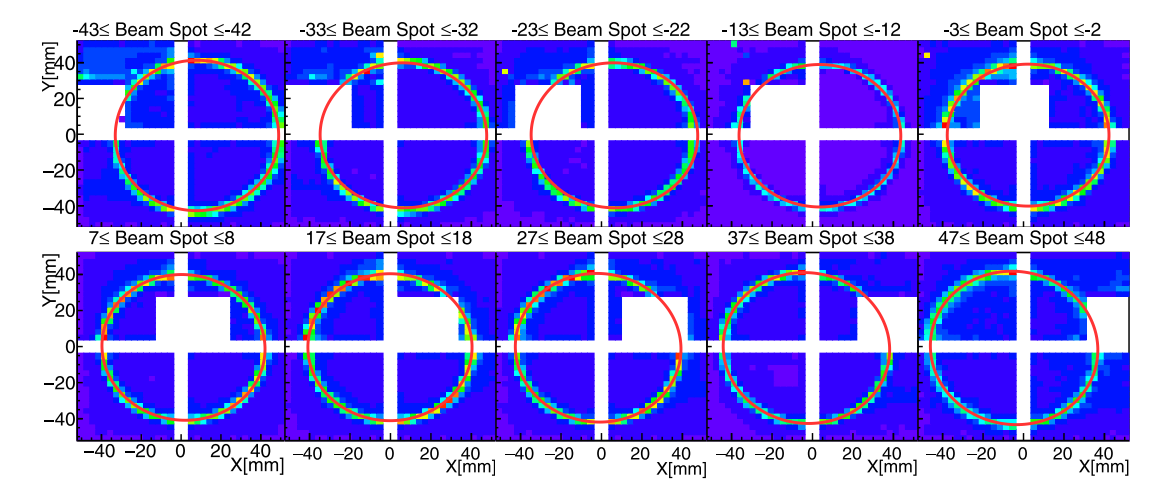


Fig. 4. Ellipse fits to cumulative rings for different beam hit positions. These fits are used to extract initial parameters for an event-by-event fitting procedure. The area around the beam spot position is masked, the white area in the above panels, during the fitting since it biases the fit procedure.

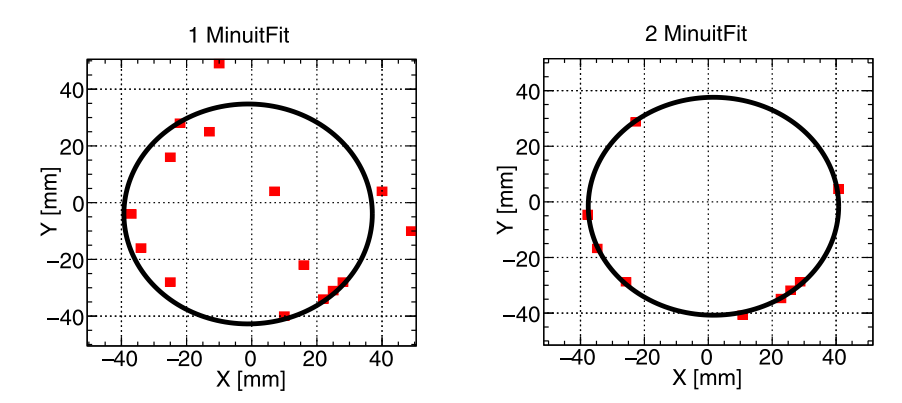


Fig. 5. Example of iterative fitting procedure for one single event. The left panel shows the photon hits seen for one event in mRICH, and the first iteration of TMinuitFit. The right panel shows the hits that survive 4σ cut based on the first fitted ellipse and the final fitted ellipse using the survived photon hits.

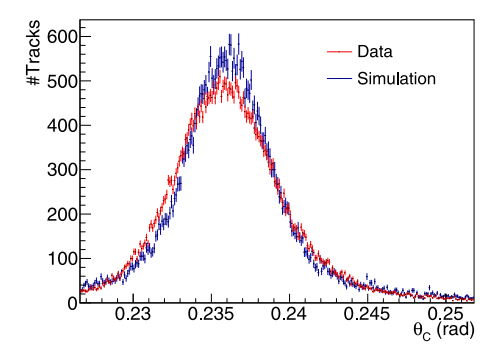


Fig. 6. Reconstructed Cherenkov angle distribution for the tracks that fall on the surface of the aerogel within -6 < X < -7 mm and 15 < Y < 16 mm for data (red) and simulation (blue).

done with the photon hits that are more than 4σ away from the fit being removed from the pool of photons used for the successive iteration. This process is continued until the fit results are stable, and we take the average of major and minor radii of this final fit as the approximation for the radius, r_0 , of the Cherenkov ring on the sensor. Fig. 5 shows the process of masking hits and iterative fit procedure for one event. For this event, as is the case for most of the events, once photon hits based on expected ring position are masked the fit converges after one

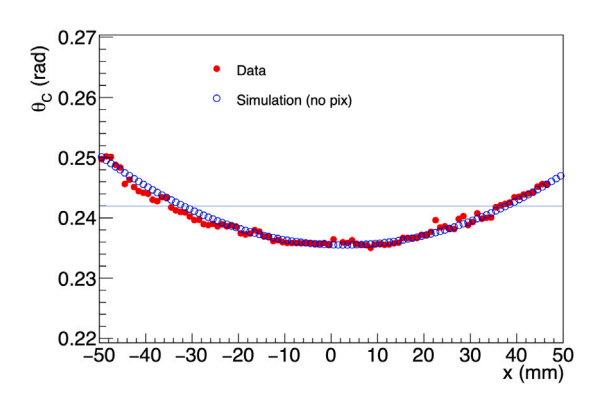


Fig. 7. Reconstructed Cherenkov angle as a function of the horizontal position of the beam at the aerogel block for the data (solid red circles) and simulation (blue circles). The solid line shows truth Cherenkov angle from the aerogel at n = 1.03.

or two iterations. The initial seed values of the fit parameters used in this procedure are taken from cumulative ring image fits derived as a function of track position on the aerogel, as shown in Fig. 4.

The Cherenkov angle resolution (σ_{θ_C}) is derived from the width of Cherenkov angle (θ_C) distribution, with θ_C calculated from radius r_0

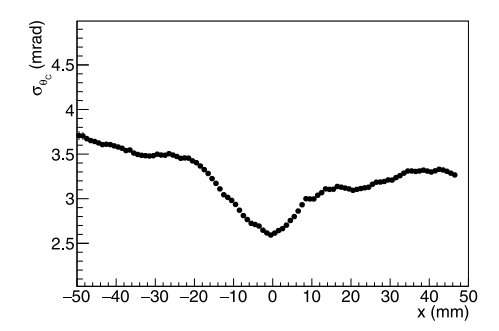


Fig. 8. Reconstructed Cherenkov angle resolution as a function of the horizontal position of the beam at the aerogel block.

according to the following equation,

$$\theta_c = \sin^{-1} \frac{r_0}{n\sqrt{r_0^2 + f^2}} \,, \tag{1}$$

where f is the focal length of Fresnel lens and n=1.03 is the index of refraction of the aerogel. As an example, Fig. 6 shows the distributions of reconstructed Cherenkov angle for the tracks that fall on the surface of the aerogel within -6 < X < -7 mm and 15 < Y < 16 mm for data and simulation. The resulting reconstructed Cherenkov angle is shown in Fig. 7 and its resolution (σ_{θ_C}) is shown in Fig. 8. Fig. 9 shows the reconstructed Cherenkov angle distribution for fixed number of photons (N_Y) on the ring, at X = 46.5 mm.

The single photon resolution, σ_{θ} , is extracted by fitting the distribution of σ_{θ_C} as a function of number of photons on the ring, N_{γ} ,

according to Eq. (2).

$$\sigma_{\theta_c}^2 = \left(\frac{\sigma_{\theta}}{\sqrt{N_{\gamma}}}\right)^2 + \sigma_{Glob}^2 , \qquad (2)$$

where σ_{Glob} accounts for possible systematic errors that do not correlate with N_γ . The term σ_{Glob} combines all contributions that are independent of the single photon measurement. These include misalignment of the photon detector modules, the resolution determination due to multiple scattering and background hits and errors in the calculation of the reconstructed track parameters. For the single photon angular resolution, the typical contributions to be considered include:

$$\sigma_{\theta}^2 = \sigma_{EP}^2 + \sigma_{Chro}^2 + \sigma_{Det}^2 \,, \tag{3}$$

where σ_{EP} is the geometrical error related to the emission point; σ_{Chro} is the error due to the chromatic dispersion of the radiator; and σ_{Det} is the error introduced by the finite pixel size of the photon detector. σ_{EP} is minimized at the focal plane of the lens, and σ_{Chro} is reduced by ultraviolet (UV) filtering (acrylic lens). As an example, a fit of σ_{θ_C} versus N_γ for electron tracks hitting the aerogel at approximately 46.5 mm is shown in Fig. 10. Fig. 11 shows σ_θ at different positions along the horizontal beam profile by repeating the above procedure for each of the *X*-positions in 1 mm bins.

A detailed Geant4 simulation of the mRICH prototype has been developed [7]. The JLab secondary beam is simulated by 3 GeV/c electrons with a smeared X-Y position by 50 μ m to account for the resolution of the GEM trackers. Along the horizontal axis, a divergence of 1° at -5.0 cm linearly decreasing to 0° at 5.0 cm is assigned to match what is observed in the data.

Fig. 12 shows a simulated event display of a 3 GeV/c electron incident at the front of the aerogel. Similar to the data, the event-by-event distributions of Chernkov photons on the sensor plane were fitted

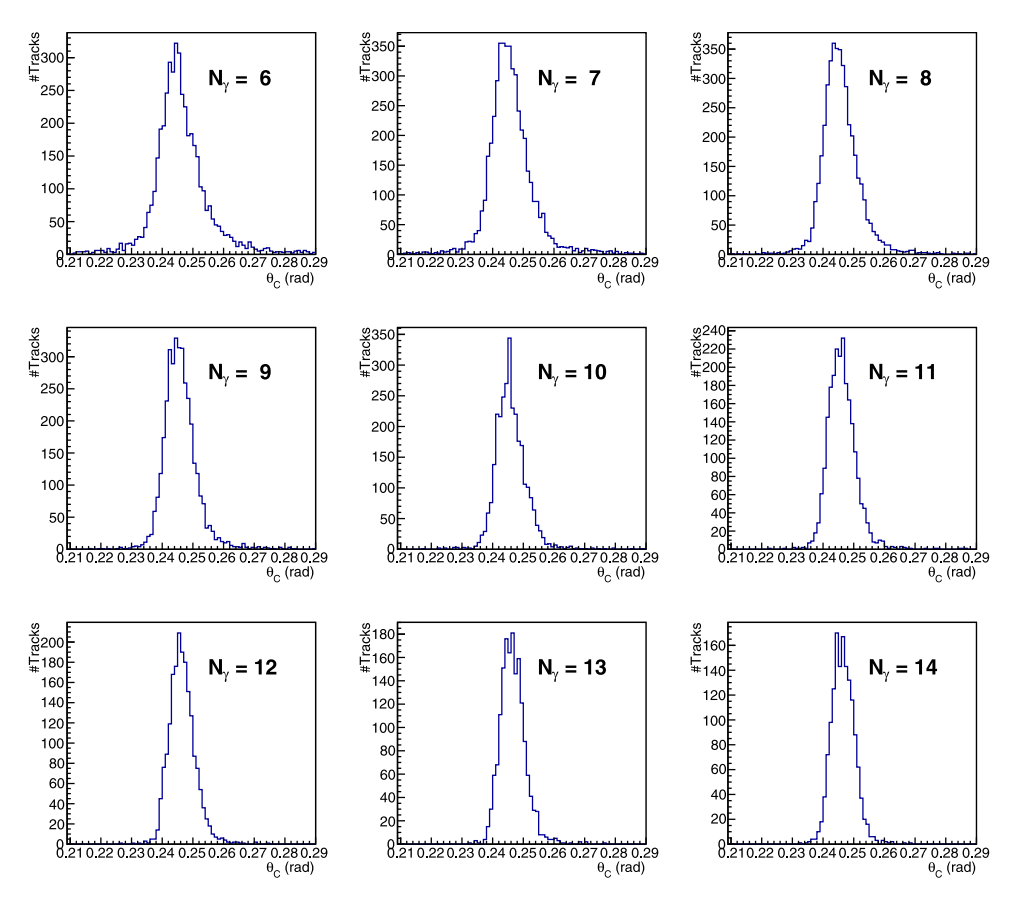


Fig. 9. Reconstructed Cherenkov angle distribution for fixed N_v , from $N_v = 6$ to $N_v = 14$, at X = 46.5 mm.

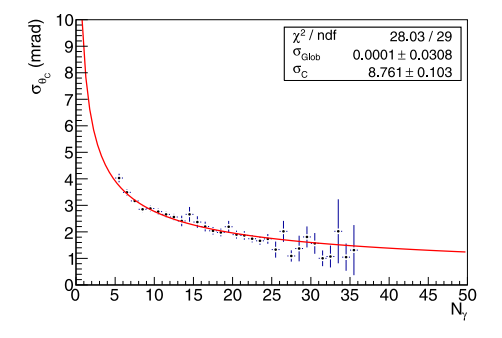


Fig. 10. Cherenkov angle resolution as a function of N_x at X = 46.5 mm.

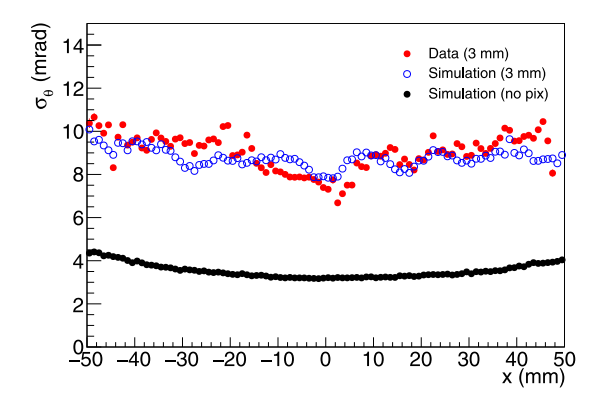


Fig. 11. Cherenkov single photon angle resolution along the horizontal position of the beam for data (solid red circles), simulation with 3 mm pixelization (blue circles), and simulation without pixelization (solid black circles).

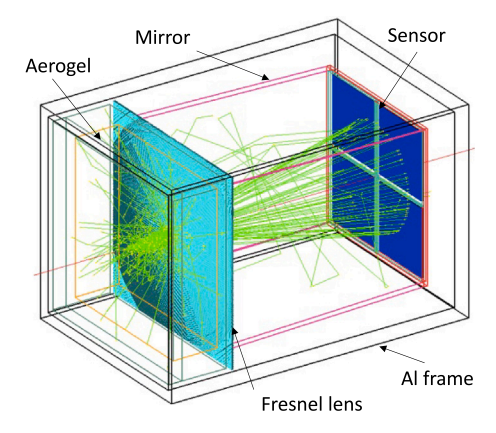


Fig. 12. A simulated event display of a 3 GeV/c electron incident at the aerogel. The various mRICH components are labeled in the figure. The figure also shows the electron (red) and the resulting Cherenkov photons (green).

by an ellipse and the radius of Cherenkov ring is taken as the average of the ellipse radii. Fig. 7 shows reconstructed Cherenkov angle from simulation for electrons incident at the aerogel along the horizontal axis. To extract the single photon resolution, a similar procedure to that of the data is followed. The results are shown in Fig. 11. The

simulation agrees with the data very well which demonstrates a proper and realistic description of the mRICH prototype in the Geant4 setup.

4. Results and discussion

The observed single photon resolution is less than 10 mrad and drops to ~ 8 mrad near the center of the aerogel block. This resolution is an improvement over what was observed with the proximity focusing RICH at 14 mrad [11]. The good agreement between the data and simulation allowed us to use the simulation to explore the various factors that contribute to the single photon resolution in mRICH design. These studies showed that the pixel size has a dominant impact on the resolution. Removing the pixelization in the simulation drastically improves the resolution to below 4 mrad and drops to ~ 3.2 mrad in the central region, as shown in Fig. 11. These simulation studies also showed that the impact of the pixel size is stronger on mRICH design than on the proximity focus design. Fresnel lens focuses Cherenkov ring near its focal point which is at a much shorter distance than the expansion volume for the proximity focus design and, therefore, at a smaller ring radius (~ 3.5 cm), i.e., 3 mm pixel size has a larger impact on 3.5 cm radius than that on 7.0 cm in the proximity focus case.

Additional effect explored by the simulation was the location of the sensor. During the beam test the sensor was located at the focal point of Fresnel lens, and a scan of the longitudinal position of the sensor in the simulation showed a strong impact on the resolution. Fig. 13(a) shows the ring radius distributions at different sensor locations relative to the focal point of Fresnel lens while Fig. 13(b) shows the width of these distributions (σ_R), which is a proxy of σ_θ . This study clearly shows that the optimal focusing position is closer to the lens by ~ 1.8 cm than the effective focal length of the 6"-Fresnel lens, and an improvement by more than a factor of 2 in σ_R is observed at the optimal focusing position, as shown in Fig. 13(b).

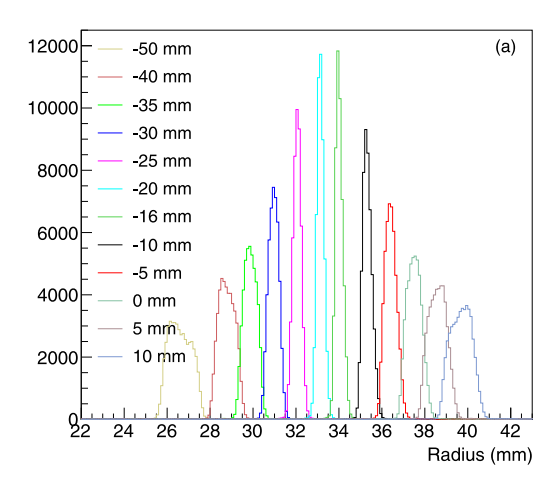
The shape of the reconstructed Cherenkov angle distribution with strong dependence on track incidence position and angle on the surface of the aerogel block, as shown in Figs. 7 and 8, indicates possible biases in the reconstructed Cherenkov angle determination. The reconstructed Cherenkov angle increases and its resolution worsens as the track approaches the edge of the aerogel black and similar effect happens as incidence angle increases. However, these effects could be due to the sensor not being located at the optimal focusing position.

While the mRICH single photon resolution is being limited by the pixel size (3 mm), the Fresnel lens focusing and re-centering coupled with the modular design enables using the log likelihood PID method for π/K separation very effectively with a reach of 3σ separation for momenta beyond 8 GeV/c, as demonstrated in the Yellow Report [1] and ECCE proposal [3]. It is also worth noting that being limited by the pixel size is a positive aspect of mRICH since the sensor technologies are advancing very quickly which opens the window for further improvement on the resolution and, consequently, its momentum reach.

5. Summary and outlook

A prototype of a modular RICH detector with two GEM trackers has been successfully tested at JLab. We observed a single photon resolution of < 10 mrad; however, this resolution is dominated by the pixel size and the position of the sensors relative to the lens. The position of the sensors was not at the optimal focusing position, and simulations showed that an improvement in the resolution by more than a factor of two is possible. This improvement is before taking the pixel size into account.

We are currently planning for another beam test to study the impact of optimal focusing position on the single photon resolution.



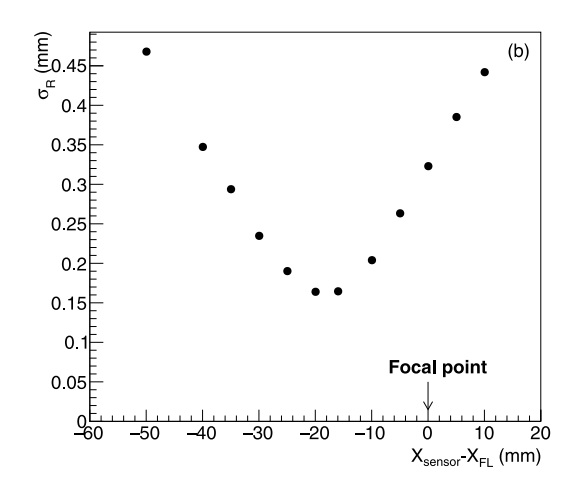


Fig. 13. (a) The simulated ring radius distribution for different sensor locations relative to the focal point of Fresnel lens. (b) The widths of the simulated ring radius distributions (σ_R) as a function of sensor location. The *x*-axis in (b) indicates the difference between the position of the sensor and the focal plane of the lens.

CRediT authorship contribution statement

D. Sharma: Formal analysis, Software, Data curation, Writing – original draft. L. Barion: Resources. M. Contalbrigo: Resources. K. Gnanvo: Resources, Software. X. He: Funding acquisition, Project administration, Supervision, Data curation, Writing – original draft. Y. Ilieva: Resources. B. Karki: Resources, Data curation. M. Sarsour: Formal analysis, Funding acquisition, Investigation, Software, Writing – original draft, Writing – review & editing. Z.W. Zhao: Resources, Software, Data curation.

Declaration of competing interest

The authors declare that they have no known competing financial interests or personal relationships that could have appeared to influence the work reported in this paper.

Data availability

Data will be made available on request.

Acknowledgments

We wish to thank the JLab Hall-D staff for their assistance with the secondary electron beam operation. We also want to thank the staff of the Instrument Shop at Georgia State University for their assistance in constructing the prototype detector. This work was partially supported with the EIC R&D funding from the Office of Nuclear Physics in the Office of Science of the Department of Energy, USA.

References

- R. Abdul Khalek, et al., Science requirements and detector concepts for the electron-ion collider: EIC Yellow Report, Nuclear Phys. A 1026 (2022) 122447, http://dx.doi.org/10.1016/j.nuclphysa.2022.122447.
- [2] J. Adam, et al., ATHENA detector proposal a totally hermetic electron nucleus apparatus proposed for IP6 at the Electron-Ion Collider, J. Instrum. 17 (10) (2022) P10019, http://dx.doi.org/10.1088/1748-0221/17/10/P10019.
- [3] J.K. Adkins, et al., Design of the ECCE detector for the electron ion collider, 2023.
- [4] T. Iijima, et al., A novel type of proximity focusing RICH counter with multiple refractive index aerogel radiator, Nucl. Instrum. Methods Phys. Res. A 548 (3) (2005) 383–390, http://dx.doi.org/10.1016/j.nima.2005.05.030.
- [5] R. Pestotnik, et al., Aerogel RICH for forward PID at Belle II, Nucl. Instrum. Methods Phys. Res. A 732 (2013) 371–374, http://dx.doi.org/10.1016/j.nima. 2013.06.080, Vienna Conference on Instrumentation 2013.
- [6] C. Wong, et al., Modular focusing ring imaging Cherenkov detector for electronion collider experiments, Nucl. Instrum. Methods Phys. Res. A 871 (2017) 13–19, http://dx.doi.org/10.1016/j.nima.2017.07.001.
- S. Agostinelli, et al., Geant4—A simulation toolkit, Nucl. Instrum. Methods Phys.
 Res. A 506 (3) (2003) 250–303, http://dx.doi.org/10.1016/S0168-9002(03) 01368-8.
- [8] C. Altunbas, M. Capéans, K. Dehmelt, J. Ehlers, J. Friedrich, I. Konorov, A. Gandi, S. Kappler, B. Ketzer, R. De Oliveira, S. Paul, A. Placci, L. Ropelewski, F. Sauli, F. Simon, M. van Stenis, Construction, test and commissioning of the triple-gem tracking detector for compass, Nucl. Instrum. Methods Phys. Res. A 490 (1) (2002) 177–203, http://dx.doi.org/10.1016/S0168-9002(02)00910-5.
- [9] M.J. French, et al., Design and results from the APV25, a deep sub-micron CMOS front-end chip for the CMS tracker, Nucl. Instrum. Methods Phys. Res. A 466 (2001) 359–365, http://dx.doi.org/10.1016/S0168-9002(01)00589-7.
- [10] S. Martoiu, H. Muller, J. Toledo, Front-end electronics for the Scalable Readout System of RD51, in: 2011 IEEE Nuclear Science Symposium Conference Record, 2011, pp. 2036–2038, http://dx.doi.org/10.1109/NSSMIC.2011.6154414.
- [11] S. Iwata, et al., Particle identification performance of the prototype aerogel RICH counter for the Belle II experiment, Prog. Theor. Exp. Phys. 2016 (3) (2016) http://dx.doi.org/10.1093/ptep/ptw005, 033H01.